Макрогетероциклы
http://mhc-isuct.ru

DOI: 10.6060/mhc256745z

Experimental and Theoretical Determination of the Main Types of Ligands in a Mixture of Petroporphyrins

Yuriy A. Zhabanov,[a,b@] Georgiy L. Pakhomov,[a,c] Vladislav V. Travkin,[a,c] Dmitry A. Vyalkin,[b] Ekaterina D. Rychikhina,[a,b] Nikolay A. Mironov,[a] and Makhmut R. Yakubov[a]

[a]*Arbuzov Institute of Organic and Physical Chemistry RAS, 420029 Kazan, Russian Federation*
[b]*Ivanovo State University of Chemistry and Technology, 153000 Ivanovo, Russian Federation*
[c]*Institute for Physics of Microstructures of the Russian Academy of Sciences (IPM RAS), 603087 Nizhny Novgorod, Russian Federation*
[@]*E-mail: zhabanov@isuct.ru*

A combination of computational modeling and experimental techniques was used to study metal-porphyrin complexes containing in crude oil (petroporphyrins). The TDDFT method was applied to calculate the electronic absorption spectra of vanadyl and nickel petroporphyrin complexes. A correlation was established between the ligand structure and the characteristics of B- and Q-absorption bands. The permanent electric dipole moments of the petroporphyrin complexes were shown to differ from each other by a factor of six. The simulated spectrum of the vanadyl-porphyrin mixture was found to closely match the experimental spectrum of the sample solution isolated from the asphaltene fraction of crude oil, enabling prediction of the electronic absorption spectra of mixtures with a known ligand composition. The sublimation of the petroporphyrin mixture under high vacuum conditions was experimentally investigated by two methods: evaporation from a Knudsen cell with in-situ mass spectrometric detection and sublimation from a quartz crucible with ex-situ recording of the sublimate absorption spectra. In both cases, the composition of the vapor above the analyzed petroporphyrin mixture depended on the process time and temperature. This result opens up new opportunities for separating petroleum porphyrin mixtures into their individual components and producing thin films with controlled properties.

Keywords: Petroporphyrins, quantum chemistry, absorption spectra, high-temperature mass spectrometry, sublimation, films.

Экспериментальное и теоретическое определение основных типов лигандов в смеси петропорфиринов

Ю. А. Жабанов,[a,b@] Г. Л. Пахомов,[a,c] В. В. Травкин,[a,c] Д. А. Вьялкин,[b] Е. Д. Рычихина,[a,b] Н. А. Миронов,[a] М. Р. Якубов[a]

[a]*Институт органической и физической химии имени А.Е. Арбузова Казанского научного центра РАН, 420029 Казань, Российская Федерация*
[b]*ФГБОУ ВО Ивановский государственный химико-технологический университет, 153000 Иваново, Российская Федерация*
[c]*Институт физики микроструктур РАН, 603087 Нижний Новгород, Российская Федерация*
[@]*E-mail: zhabanov@isuct.ru*

Проведено исследование металлокомплексов порфиринов, содержащихся в нефти (петропорфиринов), с использованием компьютерного моделирования и экспериментальных методов. Методом TDDFT рассчитаны электронные спектры поглощения для комплексов петропорфиринов с ванадилом и никелем. Установлена корреляция между строением лиганда и характеристиками B- и Q-полос поглощения. Обнаружено, что

постоянные электрические дипольные моменты комплексов могут различаться в 6 раз. Смоделированный спектр смеси ванадил-порфиринов хорошо согласуется с экспериментальным спектром раствора образца, выделенного из асфальтеновой фракции нефти, что позволяет прогнозировать электронные спектры поглощения смесей при известном лигандном составе. Экспериментально изучен процесс сублимации смеси петропорфиринов в условиях высокого вакуума. Использовались два метода: испарение из ячейки Кнудсена с in-situ масс-спектрометрией и из трубчатого тигля с ex-situ регистрацией спектров поглощения сублимата. В обоих случаях состав пара над смесью петропорфиринов зависел от времени и температуры, что открывает возможности для разделения сложных смесей на индивидуальные компоненты и получения тонких плёнок с заданными свойствами.

Ключевые слова: Петропорфирины, квантовая химия, спектры поглощения, высокотемпературная масс-спектрометрия, сублимация, пленки.

Introduction

Metal complexes of tetrapyrrolic macrocycles contained in crude oil (also known as petroporphyrins) can be isolated only as mixtures. Each mixture contains several types of tetrapyrrolic ligands with different peripheral substituents, the ratio of which depends on the origin of the oil feedstock. The most common types are alkane-type (etioporphyrins, Etio), cycloalkane-type (deoxyphylloerythroetioporphyrins, DPEP), and benzo- or rhodo-type (Rhodo); their combinations within the same ligand are also possible.[1–10] The chemical structures of the compounds are shown in Figures 1 and 2. Further separation of the mixtures into isomerically pure single-component products – for example, the isolation of a pure vanadyl Rhodo-porphyrin – remains a challenging and largely unsolved problem.[7,11]

In petroleum refining processes, petroporphyrins are undesirable because they poison cracking catalysts.[12,13] Moreover, vanadyl porphyrins are involved in the asphaltene aggregation, which leads to instability of petroleum dispersions during oil production and transportation.[4,14] Therefore, even with modern refining processes, petroporphyrins remain in heavy oil residues that are then used to produce boiler fuels or industrial bitumens.[15,16] Several successful attempts have been made to demetallate petroleum vanadyl porphyrins and to obtain their transition metal complexes for catalytic activity studies.[17] As shown recently, vanadyl petroporphyrins can be reversibly converted into thiovanadyl porphyrins during high-temperature processing of heavy crude oil.[18] In the case of vanadium-rich feedstocks, efficient isolation of VO-petroporphyrins may serve as an approach to obtaining high-purity petroleum materials (precursors), and with further development may lead to the production of isomerically pure metal complexes.[11] However, there is no practically significant information about the use or further functionalization of petroporphyrins thus far.

In petroleum feedstocks, most porphyrins-type ligands form complexes with vanadium(IV) or nickel(II), while complexes with other metals, such as copper(II), are rarely detected.[19] Notably, the content of V or Ni in the environment is much lower than that of iron or magnesium, which are chelated in similar tetrapyrrolic macrocycles, such as heme or chlorophyll.[4] The chemical transformation of these natural compounds into petroporphyrins underlies the biogenic theory of oil origin. This also indicates high chemical and thermodynamic stability and/or selectivity of formation of V(IV)O and Ni(II) complexes under geochemical conditions. Surprisingly, there are no data on the thermal or electrochemical (redox) stability of pure metalloporphyrins isolated from crude oil.

UV-Vis absorption spectra of different types of petroporphyrin ligands in common solvents are known to be somewhat different from each other, mainly in the shape and position of the weak Q-bands.[1,6,7] Nevertheless, electronic absorption spectroscopy is the simplest and most popular technique for rapid evaluation of petroporphyrin content/ligand ratios in crude oil extracts [1,3,5-8,20-22] but not the most accurate. Modern quantum-chemical methods, including DFT[9] and QTAIM, confirm that the structure of peripheral substituents, as well as the nature of the central ion and aromaticity of the porphyrin macrocycle, significantly influences both the electronic structure and stability of metalloporphyrins.[2] In particular, oxovanadium(IV) porphyrins exhibit greater stability than Ni(II)-containing analogues due to the higher electron density and increased N…V bond order. The N…Ni bonds, on the contrary, are more covalent but less stable because of the smaller contribution of π-bond character and lower bond strength. These features explain the high stability of VO-porphyrins and their predominance in heavy oil residues.[2] In previous works, we studied the molecular structure and solid-state properties of two synthetic petroporphyrins VO-EtioP-III and Ni-EtioP-III both experimentally and theoretically using TDDFT calculations.[23-26]

Another, more powerful technique for analyzing petroporphyrin mixtures is mass spectrometry (MS), with various enhancements for better resolution.[1,6,7,27,28] These methods allow the composition of VO(IV)- and Ni(II)-containing petroporphyrins to be determined directly in the petroleum matrix, without preliminary separation of the mixture into components. Moreover, this technique allows the molecular structure of petroporphyrins to be identified by the double bound equivalent and the number of carbon atoms in the macrocycle.[6]

In the present work, the electronic absorption spectra of the vanadyl petroporphyrin mixture isolated from sour crude oil (High-Sulfur Crude Oil Treatment Plant “Andreevka”, PJSC Tatneft) were computed using quantum-chemical methods (DFT and TDDFT) and compared with the experimentally obtained data. Mass spectrometric analysis of this mixture in the gas phase was carried out. The obtained results can be useful for the analysis of structural types of petroporphyrins and their further application as photoactive materials.[23,24]

Experimental Section and Computational Details

The petroporphyrin mixture was isolated from heavy oil asphaltenes (High-Sulfur Crude Oil Treatment Plant "Andreevka", PAO Tatneft) using a combination of extraction and chromatographic procedures. At first, the asphaltenes were separated from the heavy oil through treatment with a 20-fold *n*-hexane excess, followed by purification from co-precipitated resins with *n*-hexane on a Soxhlet extractor. Then, a DMF extract of asphaltenes was prepared by extraction and precipitation methods.[29] The extract was fractionated by column chromatography on wetted silica gel as the adsorbent and benzene as the eluent, yielding a primary concentrate of vanadyl porphyrins.[30] Then, pure vanadyl petroporphyrin fraction was isolated from this concentrate by eluting it with chloroform through a chromatographic column filled with silica sulfocationite.[31]

The resulting fine powder was evaporated from a molybdenum effusion cell, with the evaporation area/effusion orifice area ratio equal to 1000 and the orifice diameter of 1 mm. Before the procedure, the powder was studied by the X-ray diffraction (XRD) analysis method on a BRUKER D8 Discover diffractometer, which showed the powder was completely amorphous. The cell temperature was measured using a W-Re 5/20 tungsten-rhenium thermocouple calibrated against the melting points of tin, aluminium and silver. The measurements were made using an MI-1201 mass-spectrometer modified for thermodynamic studies. The electron ionization mass spectra were recorded in ~10^{-7} Torr vacuum at a temperature of 552 ± 2 K, ionization energy of 50 eV and accelerating voltage of 5 kV. The cathode emission current equaled I_{emis} = 0.5 mA.

The matrix-assisted laser desorption/ionization time-of-flight mass spectra were recorded on an UltraFlex III MALDI-TOF/TOF mass spectrometer (Bruker Daltonik GmbH) in the linear mode using a 355 nm Nd:YAG laser. Positively charged ions were detected. 1,8,9-Trihydroxyanthracene was used as the matrix compound. The matrix and then the analyte were deposited onto an MTP AnchorChip™ target as 1 % solutions in chloroform (0.5 μL each). The group composition of the spectrally pure vanadyl petroporphyrins was determined by identifying the signals of molecular cation-radicals $[M]^{+\cdot}$ of the Etio (*m/z* 459 + 14n), DPEP (*m/z* 457 + 14n), diDPEP (*m/z* 455 + 14n), Rhodo (*m/z* 453 + 14n), DPEP-Rhodo (*m/z* 451 + 14n), and diDPEP-Rhodo (*m/z* 449 + 14n) types in their mass spectra (n is an integer from 0 to 17). The relative content of these vanadyl petroporphyrin types was calculated from the peak intensities of the respective homologues detected in the mass spectra.

Additionally, the mixture of petroporphyrins was sublimated in a customized VUP-5M station under approximately the same vacuum conditions but the molybdenum cell was substituted for a quartz crucible with resistive heating from room temperature (RT) to the sublimation onset point (T_{subl}). Since the preliminary tests showed that the sublimation temperature range for this mixture was quite broad – from 170 to 270 °C, the experiments were conducted at three fixed temperature points: 175 ± 5, 215 ± 5 and 255 ± 5 °C, at which the material evaporated continuously from the crucible. After the selected temperature was reached, the shutter above the crucible was opened, and the sublimated material was deposited as a thin layer (~20 nm) onto functional transparent substrates (glass/ITO/MoO_3),[9,11] which was followed by measurements of the UV-Vis absorption spectra.

Geometry optimization and subsequent computation of harmonic vibrations for the metal-free petroporphyrins (Etio, DPEP, diDPEP, Rhodo, Rhodo-DPEP, and Rhodo-diDPEP types) and their vanadyl and nickel complexes were carried out using the DFT composite method r^2SCAN-3c.[32] The NICS aromaticity indices[33] were computed for all the above-mentioned molecules applying the GIAO method.[34-36] The theoretical electronic absorption spectra of the vanadyl and nickel petroporphyrin complexes were simulated within TDDFT approximation (CAM-B3LYP[37]/def2-TZVP[38]) for 50 excited states. The effects of the solvent (chloroform) were taken into account by applying the CPCM model. All the calculations were performed in the ORCA 5.0 program package.[39] The *Supporting Information* section provides the systematic IUPAC names of all the compounds discussed in the present study.

Results and Discussion

Molecular structure and absorption spectra

Quantum chemical calculations for the petroporphyrin complexes were initiated from geometries derived from single-crystal X-ray diffraction (SC-XRD) data.[21,22,40–42] For both Etio- and DPEP-type complexes, the optimized structures successfully reproduced the experimental macrocycle distortion patterns and substituent orientations, even though the computed internuclear distances and bond angles showed minor deviations. For example, the Ni(II)-DPEP macrocycle had a ruffling distortion, while VO(IV)-DPEP adopted a domed conformation associated with the presence of an axial ligand. The calculated bond length values in both cases were higher than those from the SC-XRD analysis, but the deviation did not exceed 0.03 Å.

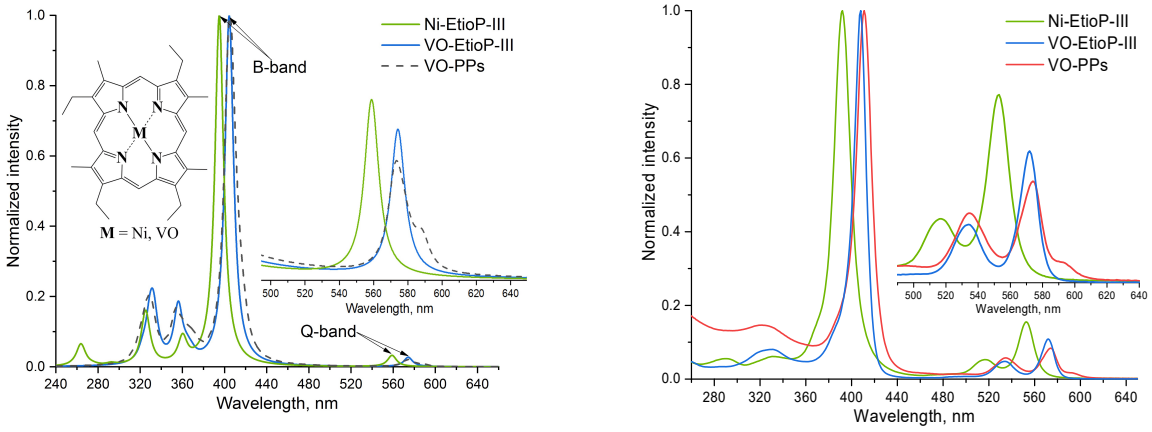

Figure 1. Comparison of the absorption spectra of VO(IV)-EtioP-III, Ni(II)-EtioP-III, and the mixture of vanadyl petroporphyrin complexes VO-PPs: (a) spectra simulated based on TDDFT calculations; (b) experimental UV-Vis spectra for solutions in chloroform (the spectra are shown for the same compounds as those used in Ref.,[23] but recorded with higher accuracy and over a broader wavelength range). The calculated spectra are shifted by 60 nm for convenience of comparison of the absorption band profiles.

Figure 1 presents the calculated (a) and experimental (b) absorption spectra of the nickel and vanadyl Etio-type complexes. The experimental spectra were recorded for dilute solutions of the complexes, which were synthesized and fully characterized, including by single-crystal X-ray diffraction, as described previously.[23,24]

As is seen in Figure 1, both the calculated and experimental spectra show a bathochromic shift of the Q- and B-bands when Ni(II) in EtioP-III is replaced by VO(IV). Analysis of metalloporphyrin spectra[43-45] reveals that the bathochromic shift of the Q-band can be attributed to the larger coordination cavity in the latter. Since the Q-band corresponds mainly to the HOMO→LUMO electronic transition (Tables S1, S2), its position correlates with the HOMO-LUMO energy gap. An increase in the size of the porphyrin coordination cavity results in greater stabilization of the LUMO compared to the HOMO, because both frontier orbitals are localized on the porphyrin macrocycle, whereas the LUMO is antibonding in nature (Figure 3). The size of the coordination cavity can be characterized by the N…N internuclear distance between the opposite pyrrolic nitrogen atoms. According to our quantum chemical calculations, this value for VO(IV)-EtioP-III is 0.14 Å higher than that for Ni(II)-EtioP-III, whereas the HOMO-LUMO energy gap in the former is 0.07 eV smaller, which causes the observed bathochromic shift of the absorption bands.

As described earlier,[23] the mixture isolated from crude oil contains only vanadyl porphyrins without detectable amounts of nickel complexes. This conclusion is supported by the close similarity between the calculated and experimental spectra of VO-PPs and VO(IV)-EtioP-III, as well as from their clear distinction from the spectra of pure Ni(II)-EtioP-III. However, the similarity is incomplete: while the shift of λ_{max} for the B-band is nearly negligible (within 2 nm), the Q-band region of VO-PPs shows a change in the relative intensity of the doublet, a weak bathochromic shift of *ca.* 4 nm, and an additional absorption shoulder at longer wavelengths with λ_{max}~592 nm (see the inset in Figure 1b).

Figure 2 shows the calculated electronic absorption spectra of the other two petroporphyrin types containing DPEP- and Rhodo-ligands, with the former one presented in its three most common variants: diDPEP, DPEP-Rhodo, and diDPEP-Rhodo. In this study, we did not use our own isomerically pure synthetic DPEP- and Rhodo-type complexes (since it was beyond the scope of this study), which could serve as the reference samples as in case of VO(IV)-EtioP-III and Ni(II)-EtioP-III. The VO(IV)-/Ni(II)-DPEP[13,22,46] and VO(IV)-Rhodo[42,47] synthesis procedures have been described earlier, and we used the data on the electronic absorption spectra from elsewhere.[22,47] These data are shown by dashed lines in Figure 2.

The spectra simulated based on the TDDFT calculations for the metal complexes with DPEP- and Etio-type ligands are almost identical (cf. Figures 1a and 2a), indicating that the presence of an exocyclic fragment in the ligand has only a minor effect on the electronic structure of the macrocyclic ring. For example, in DPEP complexes, the bathochromic shift of the B-band is only 3 nm, whereas that of the Q-band is 1 nm, which is too small to be visible in the experimental spectra,[22,23] because these values are within the instrumental error. In the Rhodo-type complexes, in contrast to the DPEP- or Etio-types, the bathochromic shift of the B-band equals 10 nm and that of the Q-band is as great as 14 nm. In addition, the Rhodo-type structures exhibit increased oscillator strength and splitting of the Q-band (Figure 2b). The latter is related to the electronic transitions involving molecular orbitals that partially extend to the benzene fragment and corresponding to shorter wavelengths relative to the Q-band position (518-529 nm). The main contribution to the Q-band formation originates from the HOMO→LUMO transitions, which is typical of porphyrins and was described in Gouterman's works.[40,48] In the Rhodo-type structures, the Q-band splitting is caused by transitions with slightly lower oscillator strengths between the orbitals: HOMO–1→LUMO and HOMO→LUMO+1 (Tables S1, S2; Figures S2, S3).

The B-band in the Rhodo-porphyrin spectra is also split (Figure 2b). The origin of this splitting is similar to that for the Q-band. For example, in case of VO(IV)-DPEP, the main contribution to the B-band arises from the transitions to excited states 14 and 15, which correspond to 347 and 345 nm (Table S2). It is evident that the 2 nm difference cannot cause band splitting. And in case of VO(IV)-Rhodo, the dominant contribution to the B-band comes from the transitions to electronic states 13 and 15, which correspond to the wavelengths of 353 and 345 nm (Table S2). Notably, electronic excited state 15 mainly results from the HOMO→LUMO+1 transition. The shapes of the LUMO and LUMO+1 orbitals in VO(IV)-Rhodo are nearly identical, except that LUMO+1 is extends to the benzene fragment (Figure S3). In case of the DPEP-type structures, the LUMO and LUMO+1 orbitals are similar in their shape and energy and can thus be called quasi-degenerate.

The Q- and B-absorption bands in the calculated spectra of the DPEP and diDPEP petroporphyrins have similar profiles (*cf.* Figures 2a and b). There is only a small (about 2 nm) bathochromic shift of the diDPEP spectra relative to those of the DPEP spectra. A comparison of the spectra of the DPEP-Rhodo and Rhodo petroporphyrins shows that the B-band for DPEP-Rhodo is not split. This can be explained by the fact that in the DPEP-Rhodo structures, both the LUMO and LUMO+1 orbitals are partially localized on the atoms of the benzene fragment, whereas in the Rhodo structures, the atomic orbitals of the benzene fragment are involved only in the formation of LUMO+1 (Figures S2, S3). Finally, in case of the diDPEP-Rhodo structures, the band is not split; instead, both the Q- and B-bands have a shoulder on the short-wavelength side.

Figure 3 shows the energy diagrams and shapes of frontier molecular orbitals of vanadyl (a) and nickel (b) petroporphyrin complexes, respectively. The HOMO-LUMO energy gaps for the Etio-, DPEP-, and diDPEP-type structures differ by no more than 0.04 eV and can be considered nearly identical. The shapes of the frontier orbitals of these three structures are also almost the same, which is the reason why their calculated spectra in Figures 1a, 2a and 2c are similar.

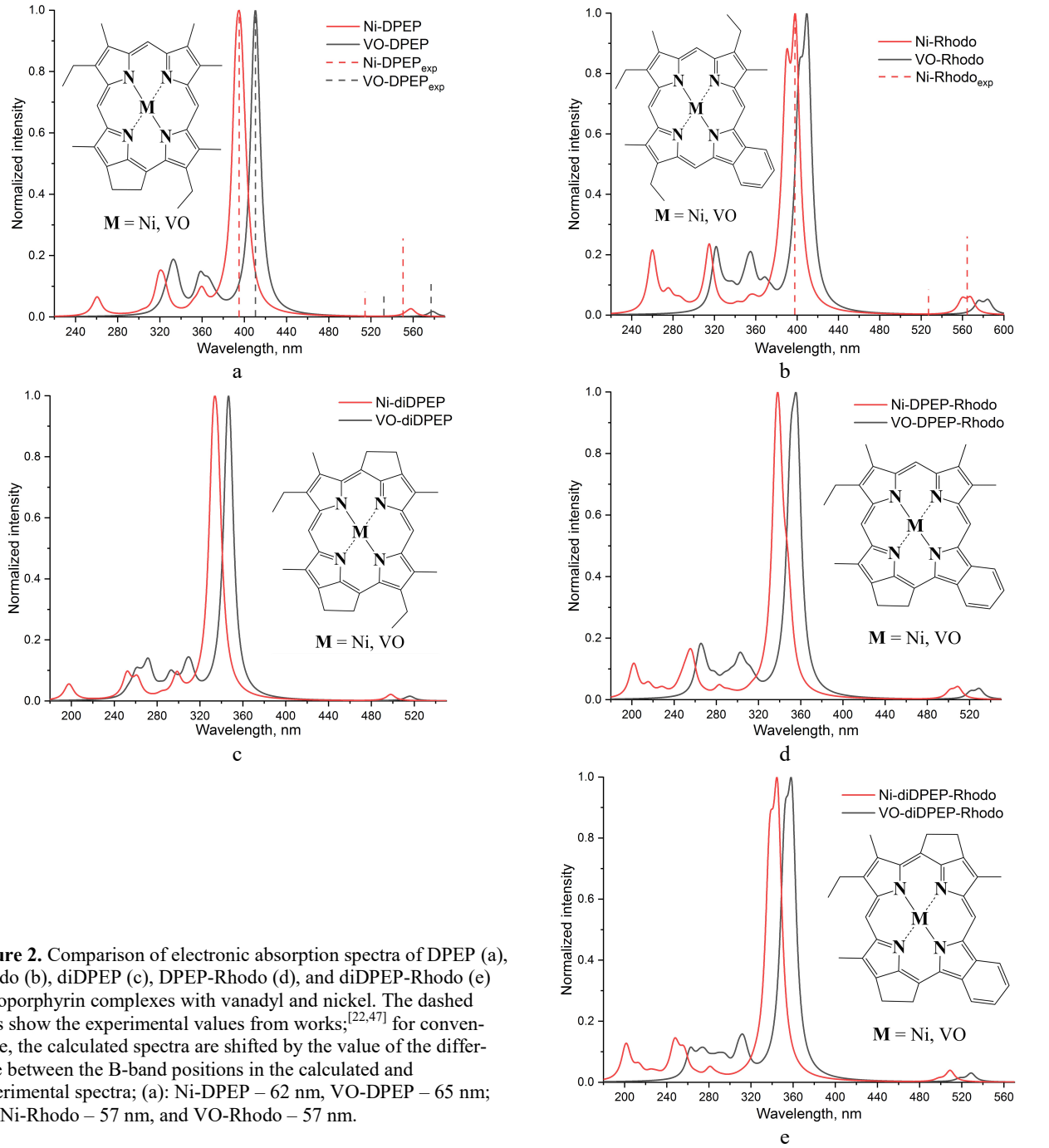

Figure 2. Comparison of electronic absorption spectra of DPEP (a), Rhodo (b), diDPEP (c), DPEP-Rhodo (d), and diDPEP-Rhodo (e) petroporphyrin complexes with vanadyl and nickel. The dashed lines show the experimental values from works;[22,47] for convenience, the calculated spectra are shifted by the value of the difference between the B-band positions in the calculated and experimental spectra; (a): Ni-DPEP – 62 nm, VO-DPEP – 65 nm; (b): Ni-Rhodo – 57 nm, and VO-Rhodo – 57 nm.

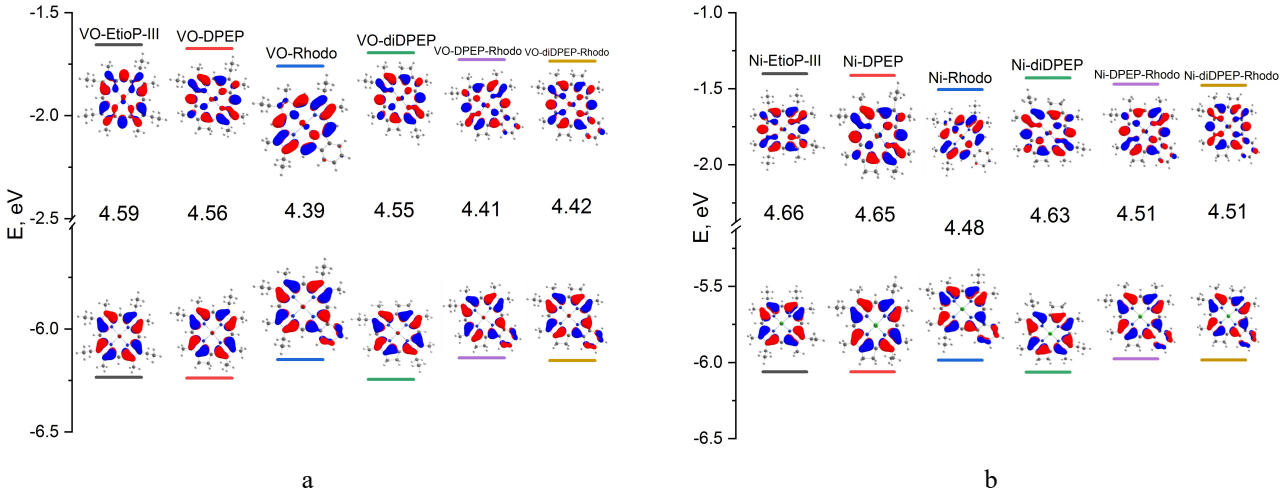

Figure 3. Diagram of the frontier molecular orbitals (MOs) and HOMO-LUMO energy gap for VO(IV)- (a) and Ni(II)-petroporphyrins (b).

However, in the Rhodo-structures, the HOMO orbitals also extend to the benzene fragments, with the HOMO-LUMO energy gap being on average 0.16 eV smaller (Figure 3). This causes a bathochromic shift of the Q- and B-bands in all the complexes with Rhodo-type ligands (see Figures 2b, d and e). Adding one or two exocyclic fragments to the original Rhodo-structure has a minor effect on the HOMO-LUMO energy gap (0.03 eV).

For different complexes of the same metal, the HOMO-LUMO energy gap is dependent solely on the ligand type. It has the minimum value for the Rhodo- and the maximum one for the Etio-type complexes (Figure 3). The difference in the energy gap values of about 0.2 eV between these extremes corresponds to a shift of *ca.* 50 nm in the Q-band region, which must be clearly seen in the available experimental reports. However, when we applied the data on the Q-band positions for the Ni(II)-EtioP-III and Ni(II)-Rhodo complexes from works[24] and [47], respectively, the shift was only 12 nm. Such difference between the calculated and experimental values resulted from the fact that CAM-B3LYP overestimates the HOMO-LUMO energy gaps by over 2 times.[49] At the same time, numerous studies have shown that the CAM-B3LYP functional provides excitation energy values and electronic spectra that are close to experimental data for a variety of compounds[48-50] including metalloporphyrin complexes.[45] It is also worth noting that the changes in the HOMO-LUMO energy gap and absolute energies of frontier molecular orbitals agree with the spectral data and cyclic voltammetry results.[22,51]

A cyclic voltammetry study was conducted for the mixture of vanadyl petroporphyrins (VO-PPs) obtained in this work. The obtained cyclic voltammogram is shown in Figure 4; the redox potentials are summarized in Table 1. The redox behavior of the VO-PPs mixture is similar to that of isomerically pure VO(IV)-EtioP-III reported previously,[23] except the additional reduction process observed at –0.74 V (Figure 1, Table 1).

In case of nickel(II) complexes, the structural trends in frontier molecular orbitals of different ligand types are analogous to those of the vanadyl complexes (Figure 3a,b). The bathochromic shift of the Q- and B-bands in VO(IV)-EtioP-III relative to Ni(II)-EtioP-III (Figure 1a) associated with the coordination cavity size has been discussed above. The diagrams in Figure 3 show that in the vanadyl petroporphyrins of the other ligand types, the HOMO→LUMO electronic transition (optical energy gap) is also less energy-demanding than in the nickel complexes with structurally similar ligands, which agrees with the experimental data, as noted earlier.[23,53]

In Figure 5, the experimental electronic absorption spectrum of the mixture of VO(IV) petroporphyrins (VO-PPs) dissolved in chloroform is compared with the calculated absorption spectra shown in Figures 1a and 1b. The spectrum of this mixture was simulated taking into account the mole fractions of the ligands: Etio – 23.6%, DPEP – 40.4%, diDPEP – 19.1%, Rhodo – 7.3%, DPEP-Rhodo – 6.0%, and diDPEP-Rhodo – 3.7%. These mole fractions were determined based on the MALDI-TOF mass spectrometry data. The calculated spectrum does not reproduce the absorption band with the maximum at ~535 nm because this band corresponds to a vibronic transition in porphyrins,[43,53] which is not treated within the TDDFT method of vertical transitions used here.

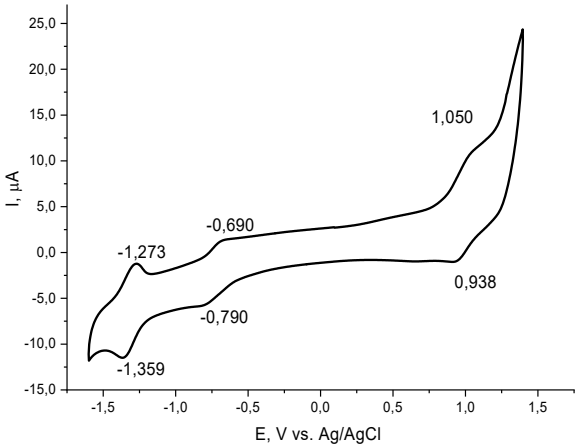

Figure 4. Cyclic voltammogram of the VO-PPs mixture in the CH_2Cl_2 solution. The scan rate is 25 mV/s.

Table 1. Redox potentials ($E_{1/2}$) in the CH_2Cl_2 solution.

Compound	$E_{1/2}^{red}$, V	$E_{1/2}^{ox}$, V
VO-PPs	-0.74 -1.32	0.99
VO-EtioP-III[22]	-1.34	1.1* 1.0

*irreversible

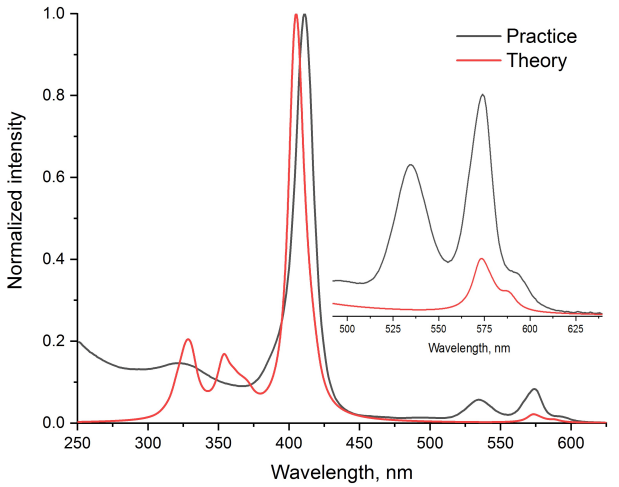

Figure 5. Comparison of the calculated and experimental absorption spectra of the VO-petroporphyrin mixture (VO-PPs).

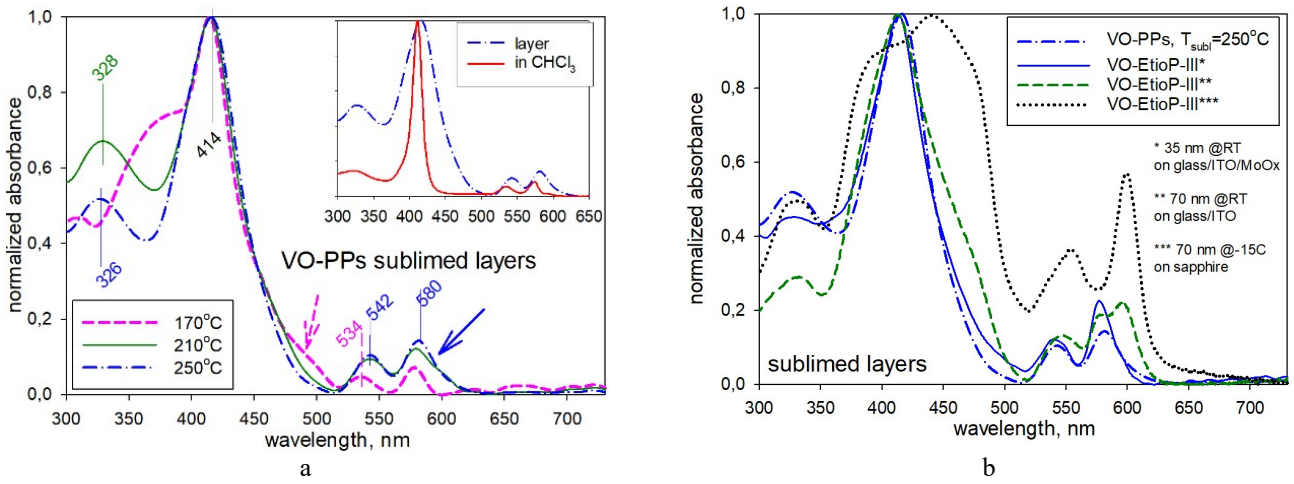

Figure 6. (a) UV-Vis spectra of thin sublimed VO-PPs layer on transparent glass/ITO/MoO_3 substrates obtained at three temperatures (T_{subl}) with sequential heating of the crucible. (b) Comparison of the UV-Vis spectrum of the thin sublimed VO-PPs layer deposited at T_{subl} = 250 °C with the spectra of the pure VO(IV)-EtioP-III layer deposited on various substrates of different thickness and temperature values during the deposition.

As Figure 5 shows, apart from this transition, the calculated and experimental absorption profiles are in good agreement within the 380–650 nm wavelength range, which is especially relevant for analytical purposes. The spectrum has an absorption band with λ_{max}= 573 nm and a shoulder in the long-wavelength region. According to the data presented above, the main peak corresponds to the Q-bands of the DPEP- and Etio-type structures, while the shoulder results from the presence of Rhodo-type structures in the mixture, the Q-bands of which are bathochromically shifted (*cf.* Figure 2). Since the fraction of the Rhodo-type structures in the mixture is small, the relative intensity of the shoulder is not high. These results allow us to suggest splitting of the Q-band in the spectrum of the mixture with a higher content of Rhodo-type ligands, with the absorption maxima at *ca.* 575 and 587 nm.

According to Refs.,[54,55] crude oil may contain porphyrins with additional heteroatoms (N, O, S) but their content does not usually exceed 10%. Mass spectrometry can only be applied to determine the content of such porphyrins if high-resolution mass spectrometers are used, which was not the case in this study. When medium-resolution mass spectrometers are used, the significant content of porphyrins with additional heteroatoms can lead to errors in the petroporphyrin content measurement due to signal overlapping. Such measurement inaccuracies may alter the profiles of the calculated absorption spectra, making them differ more significantly from the experimental ones. Therefore, the use of a comprehensive approach combining theoretical and experimental methods makes it possible to avoid inaccuracy in the petroporphyrin composition determination.

Figure 6 shows the UV-Vis spectra of VO-PPs thin films deposited on functional transparent substrates glass/ITO/MoO_3 kept at room temperature (RT) during the deposition but at different evaporation temperatures (T_{subl}) – see the Experimental section. The choice of the substrate material was dictated by the application of VO-PPs films in prototypes of photovoltaic devices (to be published elsewhere).

The UV-Vis spectra of the medium-temperature (210 °C) and high-temperature (250 °C) fractions of the VO-PPs sublimate show that the main difference between them is the lower relative intensity of the broad absorption peak in the near UV region (λ_{max} ~328 nm) and a slight dip on the long-wavelength shoulder of the Q-band (λ_{max} ~600 nm, marked with an arrow) with an increase in the T_{subl} (Figure 6a). In contrast, the spectrum of the more volatile fraction (T_{subl} = 170°C) shows distinct differences from the other two: lower Q-band intensity compared to that of the B-band with a slight hypsochromic shift, an obvious long-wavelength shoulder of the B-band in the 490–500 nm region (marked with an arrow), and, most importantly, a completely different absorption profile in the short-wavelength region (λ < 390 nm). The inset in Figure 6a compares the spectrum of the layer sublimed at T_{subl} = 250°C with that of VO-PPs in the $CHCl_3$ solution from Figures 1a and 4. It is evident that the absorption bands of the sublimate are broadened, especially the Soret band, and bathochromically shifted by 7–8 nm, which can be attributed to weak intermolecular interactions in the disordered solid phase (for details see Refs.[24,25,52,56]). The only exception is the 330 nm band where the absorption band results from transitions from lower-energy orbitals, which are less affected by the intermolecular interactions.

Figure 6b compares the spectrum of the VO-PPs layer sublimed at T_{subl} = 250°C with those of thin films of the pure (synthetic) vanadyl etioporphyrin-III, VO(IV)-EtioP-III, the only individual compound currently available to us for such a comparative test. The choice of the VO(IV)-EtioP-III films was intentional and was directed by the fact that they can be deposited under completely different conditions affecting the molecular aggregation (see Refs.[23,24]). As is seen in Figure 6b, the spectra of the VO-PPs film and the 35 nm pure VO(IV)-EtioP-III film are nearly identical, although the deposited VO-PPs mixture is expected to contain ligands of different types.

At the same time, when the VO(IV)-EtioP-III deposition conditions are favourable for the formation of ordered molecular layers (aggregates or mixed aggregate-monomer phases[22]), a strong splitting of the absorption bands is ob-

served, making the spectra of the films distinctly different from each other (Figure 6b). For example, the spectrum of the 70-nm-thick VO(IV)-EtioP-III film deposited on an ITO surface at room temperature (RT) shows a fine structure within the Q-band, whereas that of the film deposited at a negative substrate temperature indicates considerable broadening of the B-band, with the FWHM nearly 100 nm.

It is evident that the formation of aggregates in the thin film containing similar but not identical molecules in comparable (of the same order) proportions must be significantly hindered. Most likely, such film represents an amorphous matrix, unless phase segregation occurs – which would require an additional driving force, such as heating. However, in this study the substrates were not intentionally heated, and the deposited films were not annealed. Indeed, the XRD analysis revealed no evidence of long-range order in the VO-PPs films of any thickness and on any substrates, including those deposited from a solution.

Thus, in thin sublimed layers of VO(IV)-petroporphyrins, solid-state interactions can produce much stronger spectral effects than ligand composition variations. As a result, the effects of the petroporphyrin mixture composition observed in the calculated and experimental spectra may be hidden in the thin layer spectra due to absorption band broadening and shifting. Further investigation could be carried out using isomerically pure components of the mixture, such as those of the DPEP- or Rhodo-type. In the latter case, strong intermolecular interactions are more likely because Rhodo-type petroporphyrins possess the largest permanent electric dipole moment (PDM) among the compounds studied (Table 2).

Table 2. Permanent electric dipole moments (PDM) of metal-free petroporphyrins (H_2) and their nickel and vanadyl complexes obtained from quantum-chemical calculations carried out by the r^2SCAN-3c composite method, in Debye.

M	Etio	DPEP	Rhodo	di-DPEP	DPEP-Rhodo	diDPEP-Rhodo
H_2	0.45	0.52	1.13	0.25	0.67	1.08
Ni	0.42	0.59	1.20	0.23	0.85	1.24
VO	1.85	2.29	2.14	2.24	2.37	2.54

For VO-PPs with any ligand type, the presence of PDM is natural due to their nonplanar structure with an axially coordinated electronegative oxygen atom, while the situation for Ni-PPs is more complex. Therefore, we calculated the PDM values for all the considered petroporphyrin complexes, as well as their metal-free species, which are also of interest in studies of the composition of petroleum porphyrins[57–59] and their molecular structures.[11] The results are given in Table 2.

As expected, among the planar metal-free or nickel-containing molecules, the Rhodo-type with the most asymmetric conjugation system (Figure S1) has the maximum PDM value. The dipole moment of the vanadyl complexes is expectedly higher than that of the metal-free or Ni(II) complexes, but, interestingly, the highest possible PDM value among all the studied compounds is found in VO(IV)-diDPEP-Rhodo. This complex is strongly distorted into a domed conformation due to the bulky peripheral substituents of the tetrapyrrolic macrocycle (the XYZ coordinates of all the considered structures are provided in the Supporting Information). Quantitative data on the PDM values may be useful for planning chromatographic separation of petroporphyrin mixtures.

Aromaticity of petroporphyrins

In Ref.,[4] the aromaticity of petroporphyrins was studied using Bird aromaticity index for porphyrin, DPEP-, diDPEP-, and DPEP-Rhodo-type structures.[60] In the present work, the aromaticity was evaluated using the NICS criterion[33] for six of the above-mentioned metal-free petroporphyrins and their vanadyl and nickel complexes. The calculated NICS values are summarized in Table S3, and the chemical structure of the petroporphyrin with labeled rings is shown in Figure S1. According to Table S3, for the metal-free petroporphyrins, the NICS values of the pyrrole fragments containing N–H groups (rings B and D, NICS ≈ 13 ppm) are significantly higher than those of the respective rings without hydrogen (rings A and C, NICS ≈ ≈ 3 ppm), which agrees with the results reported in Ref.[4]. Metal coordination makes the electron density in the macrocyclic ring more evenly delocalized and the NICS values equal to ~6 ppm for rings A, B, C, and D in the nickel complexes and ~8 ppm in the vanadyl ones.

Alterations in pyrrole-fragment aromaticity induced by the introduction of exocyclic and/or benzene rings are more pronounced for the metalloporphyrin complexes than for the metal-free structures, though the overall trends remain the same. As expected, the NICS values for the exocycles (E and G) are close to zero. At the same time, the introduction of exocyclic fragments slightly increases (≈1 ppm) the aromaticity of the respective pyrrole rings. Thus, the effect of exocycle introduction on the aromaticity of the pyrrole fragments is similar to that of alkyl substituents (an increase in the aromaticity index upon introduction of alkyl groups was reported in Ref.[4]). In contrast, annelation with a benzene ring (F) lowers the aromaticity of the respective pyrrole ring (C) by *ca.* 2 ppm. According to Table S3, it can be concluded that the electrons of the exocycles contribute to the π-conjugation of the pyrrole rings, whereas the benzene fragments partially withdraw the electron density. Similar trends in the aromaticity of pyrrole rings in petroporphyrins were reported in Ref.[4]. The electron-withdrawing nature of the benzene fragments is also confirmed by the bathochromic shift of the Q-band when going from the Etio- to the Rhodo-type structures (Tables S1 and S2).

Composition of the vapor above the petroporphyrin mixture according to high-temperature mass spectrometry

The electron ionization mass spectra of the vapor above the petroporphyrin mixture were recorded using the Knudsen effusion cell at the temperature of 552 K. Some of the spectra are presented in Figure 7.

During the entire experiment, the ion current with the highest intensity corresponded to the molecular ion of the VO(IV)-DPEP complex (*m/z* = 541 Da, see Figure 7a). The composition of the mass spectra recorded in this work is generally similar to that reported for petroporphyrin mix-

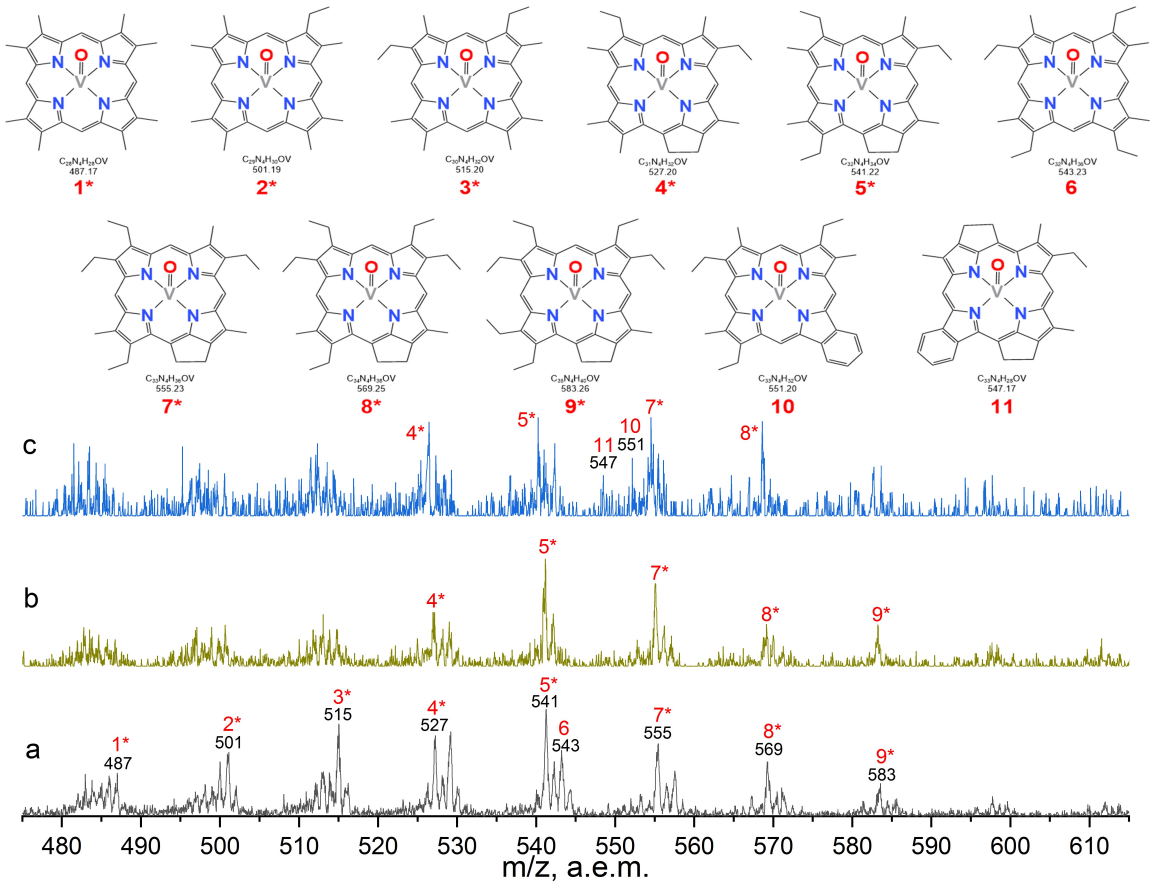

Figure 7. Electron ionization mass spectra of the petroporphyrin mixture at 552 K, recorded at the start of the experiment (a), after 1 h (b), and after 2 h (c).

tures in previous studies.[11,61] However, the relative intensities of the ion currents of the individual components changed over time, which correlates with the VO-PPs fractionation (described above) occurring during the sublimation from the crucible onto the substrate. One hour after the experiment started (Figure 7b), the relative intensity of the ion current corresponding to the molecular ion of the Etio complex (*m/z* = 543 Da) was *ca.* 10% lower than the initial value. At the same time, the relative intensity of the ion current of the DPEP-type complex with four ethyl groups (*m/z* = 555 Da) became higher than that of the DPEP-type complex with two ethyl groups (*m/z* = 527 Da). In addition, a group of low-intensity peaks (about 10%) appeared in the range of 547–551 Da corresponding to the Rhodo-type porphyrin complexes.

Two hours after the experiment started (Figure 7c), we registered a decrease in the relative intensity of the lighter molecular ion corresponding to the Etio-type porphyrin complex with two ethyl groups (*m/z* = 515 Da) and an increase in the relative intensities of the heavier molecular ions of the Rhodo-type porphyrin complexes (*m/z* = 547–551 Da) and DPEP-type porphyrin complexes with four (*m/z* = 555 Da) and five (*m/z* = 569 Da) ethyl groups. At the same time, the absolute intensity of the most intensive molecular ion peak (*m/z* = 541 Da) decreased by a factor of seven throughout the experiment. The decrease in the absolute ion intensities can be explained by the fact that, when the mixture evaporates, the total saturated vapor pressure is the sum of partial pressures of all the components, which is higher than the value required for the molecular gas flow mode assuming no collisions between the gas molecules inside the effusion cell and near the effusion orifice. Consequently, the evaporation conditions required for the Knudsen effusion method are not fully met, and the ion currents of the individual components are no longer proportional to their partial pressures.

Conclusion

In this study, we applied the TDDFT method to calculate the electronic absorption spectra of five most common types of petroleum porphyrins (DPEP, diDPEP, diDPEP-Rhodo, Rhodo, and DPEP-Rhodo) as metal-free bases and their complexes with oxovanadium and nickel, in addition to the Etio-type complexes VO(IV)-EtioP-III and Ni(II)-EtioP-III studied earlier.[23–26] We established a correlation between the number, position and intensity of the main absorption bands and the electronic structure of each ligand type, taking into account a number of factors, including the aromaticity index. The permanent electric dipole moments were determined for all possible combinations (18 molecules); their values were found to differ by factor of six within the series. These results were used to calculate the absorption spectrum of the mixture of vanadyl petroporphyrins with a known ratio of ligand types. The spectrum was then compared with the experimental UV-

Vis spectrum of the porphyrin mixture of the same composition, isolated from the asphaltene fraction by the previously developed techniques.[29–31] The good agreement between the calculated and experimental spectra in the 380–650 nm region demonstrates that changes in spectral profiles of porphyrin mixtures obtained from crude oil can be predicted from their ligand composition.

Experiments were carried out to evaporate a mixture of petroporphyrins in high vacuum using (1) a Knudsen cell and (2) a quartz crucible. In the first case, the process was accompanied by *in situ* mass spectrometric analysis of the molecular beam, and in the second case - by *ex situ* measurements of the electronic absorption spectra of the sublimed layers. In both cases, the results depended on the sublimation temperature and evaporation time, which opens up new possibilities for separating petroporphyrin mixtures into individual components and for preparing thin films with controlled physical properties.

Acknowledgements. This work was supported by the Russian Science Foundation (project No. 25-73-20101) and carried out using the equipment of the Common Research Center “Physics and Technology of Micro- and Nanostructures” at the IPM RAS. The authors are grateful to the FRC Kazan Scientific Center of RAS for the technical support of the experiments.

Author contribution. Yuriy A. Zhabanov: supervision, investigation, validation, review and editing. Georgiy L. Pakhomov: project administration, supervision, validation, conceptualization, review and editing. Vladislav V. Travkin: investigation, validation, review and editing. Dmitry A. Vyalkin: investigation, visualization, original draft. Ekaterina D. Rychikhina: investigation, visualization, original draft. Nikolay A. Mironov: investigation validation, review and editing. Makhmut R. Yakubov: investigation, resources, validation, review and editing.

References

1. Barwise A.J.G., Whitehead E.V. *Phys. Chem. Earth* **1980**, *12*, 181-192.
2. Freeman D.H., Martin D.C.S., Boreham C.J. *Energy Fuels* **1993**, *7*, 194-199.
3. Louda J.W., Baker E.W. *Initial Reports of the Deep Sea Drilling Project* **1981**, *63*, 785-818.
4. Valencia D. *Fuel* **2023**, *333*, 126344.
5. Czernuszewicz R.S. *J. Porphyrins Phthalocyanines* **2000**, *4*, 426-431.
6. Zhao X., Xu C., Shi Q. *Struct. Bond* **2015**, *168*, 39-70.
7. Yakubova S.G., Abilova G.R., Tazeeva E.G., Tazeev D.I., Mironov N.A., Milordov D.V., Yakubov M.R. *Pet. Chem.* **2022**, *62*, 83-93.
8. Baker E.W. *J. Am. Chem. Soc.* **1966**, *88*, 2311-2315.
9. Biktagirov T., Gafurov M., Mamin G., Gracheva I., Galukhin A., Orlinskii S. *Energy Fuels* **2017**, *31*, 1243-1249.
10. Malyasova A.S., Abieva F.A., Koifman O.I. *Rossiiskii Khimicheskii Zhurnal (Russ. Chem. J.)* **2023**, *67*, 104-113.
11. Zhang Y., Schulz F., Rytting B.M.K., Walters C.C., Kaiser K., Metz J.N., Harper M.R., Merchant S.S., Mennito A.S., Qian K., Kushnerick J.D., Kilpatrick P.K., Gross L. *Energy Fuels* **2019**, *33*, 6088-6097.
12. Donggun L., Ki-Duk K., Yong-Kul L. *Fuel* **2020**, 263, 116620.
13. Okunev A.G., Parkhomchuk E.V., Lysikov A.I., Parunin P.D., Semeykina V.S., Parmon V.N. *Russ. Chem. Rev.* **2015**, 84, 981-999.
14. Borisova Y.Y., Tazeeva E.G., Mironov N.A., Borisov D.N., Yakubova S.G., Abilova G.R., Sinyashin K.O., Yakubov M.R. *Energy Fuels* **2017**, *31*, 13382-13391.
15. Kamkar M., Natale G. *Fuel* **2021**, *285*, 119272.
16. Polacco G., Stastna J., Biondi D., Zanzotto L. *Curr. Opin. Colloid Interface Sci.* **2006**, *11*, 230-245.
17. Tazeev D., Musin L., Mironov N., Milordov D., Tazeeva E., Yakubova S., Yakubov M. *Catalysts* **2021**, *11*, 1506.
18. Trukhan S.N., Chibiryaev A.M., Martyanov O.N. *Energy Fuels* **2025**, *39*, 4719-4727.
19. Lesage S., Xu H., Durham L. *Hydrological Sciences Journal* **1993**, *38*, 343-354.
20. Treibs A. *Justus Liebigs Ann. Chem.* **1934**, *510*, 42-62.
21. Freeman D.H., Swahn I.D., Hambright P. *Energy Fuels* **1990**, *4*, 699-704.
22. Cantú R., Stencel J.R., Czernuszewicz R.S., Jaffé P.R., Lash T.D. *Environ. Sci. Technol*. **2000**, *34*, 192-198.
23. Rychikhina E.D., Travkin V.V., Koptyaev A.I., Gordeev K.M., Nazarov A.A., Yakubov M.R., Mironov N.A., Pakhomov G.L. *J. Porphyrins Phthalocyanines.* **2025**, *29*, 833-843.
24. Koptyaev A.I., Rychikhina E.D., Zhabanov Y.A., Travkin V.V., Pakhomov G.L. *Supramol. Mater.* **2024**, *3*, 100075.
25. Zhabanov Y.A, Eroshin A.V., Koifman O.I., Travkin V.V., Pakhomov G.L. *Macroheterocycles* **2024**, *17*, 4-8.
26. Eroshin A.V., Zhabanov Y.A., Stuzhin P.A., Pakhomov G.L. *Zh. Fiz. Khim. [Russ. J. Phys. Chem.]* **2025**, *44*, 76-87.
27. Baker E.W., Fu Yen T., Dickie J.P., Rhodes R.E., Clark L.F. *J. Am. Chem. Soc.* **1967**, *89*, 3631-3639.
28. Shaw G.J., Martin J., Quirke E., Eglinton G. *J. Chem. Soc. Perkin Trans. 1* **1978**, 1655-1659.
29. Mironov N.A., Tazeeva E.G., Milordov D.V., Abilova G.R., Tazeev D.I., Yakubova S.G., Yakubov M.R. *Russ. J. Appl. Chem.* **2021**, *94*, 1324-1333.
30. Mironov N.A., Tazeeva E.G., Milordov D.V., Yakubova S.G., Yakubov M.R. *Russ. J. Appl. Chem*. **2023**, 332-341.
31. Mironov N., Milordov D., Abilova G., Tazeeva E., Yakubova S., Yakubov M. *J. Porphyrins Phthalocyanines* **2020**, *24*, 528-537.
32. Grimme S., Hansen A., Ehlert S., Mewes J.M. *J. Chem. Phys.* **2021**, *154*, 064103.
33. Chen Zh., Wannere Ch.S., Corminboeuf C., Puchta R., von Ragué Schleyer P. *Chem. Rev.* **2005**, *105*, 3842-3888.
34. London F. *J. Phys. le Radium* **1937**, *8*, 397-409.
35. Wolinski K., Hinton J.F., Pulay P. *J. Am. Chem. Soc.* **1990**, *112*, 8251-8260.
36. Cheeseman J.R., Trucks G.W., Keith T.A., Frisch M.J. *J. Chem. Phys.* **1996**, *104*, 5497-5509.
37. Yanai T., Tew D.P., Handy N.C. *Chem. Phys. Lett.* **2004**, *393*, 51-57.
38. Weigend F., Ahlrichs R. *Phys. Chem. Chem. Phys.* **2005**, *7*, 3297-3305.
39. Neese F., Wennmohs F., Becker U., Riplinger C. *J. Chem. Phys.* **2020**; *152*, 224108.
40. Hummer D.R., Noll B.C., Hazen R.M., Downs R.T. *Am. Mineral.* **2017**, *102*, 1129-1132.
41. Ekstrom A., Fookes C.J.R., Hambley T., Loeh H.J., Miller S.A., Taylor J.C. *Nature* **1983**, *306*, 173-174.
42. Clezy P., Fookes C., Mirza A. *Aust. J. Chem.* **1977**, *30*, 1337.
43. Gouterman M. *J. Mol. Spectrosc.* **1961**, *6*, 138-163.
44. Hashimoto T., Choe Y.-K., Nakano H., Hirao K. *J. Phys. Chem. A* **1999**, *103*, 1894-1904.
45. Pan Y., Li L., Qiu F., Wei Y., Hua W., Tian G. *J. Chem. Phys.* **2019**, *150*, 164308.
46. Jeandon C., Ocampo R., Callot H.J. *Tetrahedron* **1997**, *53*, 16107-16114.

47. Boggess J.M., Czernuszewicz R.S., Lash T.D. *Org. Geochem.* **2002**, *33*, 1111-1126.
48. Gouterman M. In: *The Porphyrins* (Dolphin D., Ed.), Academic Press, **1978**, 1-165.
49. Bhatta R.S., Pellicane G., Tsige M. *Comput. Theor. Chem.* **2015**, *1070*, 14-20.
50. Rostov I.V., Amos R.D., Kobayashi R., Scalmani G., Frisch M.J. *J. Phys. Chem. B* **2010**, *114*, 5547-5555.
51. Kumar R., Kar R., Maity D.K. *J. Comput. Chem.* **2025**, *46*, e701175.
52. Pakhomov G.L., Koptyaev A.I., Yunin P.A., Somov N.V., Semeikin A.S., Rychikhina E.D., Stuzhin P.A. *Chemistry Select* **2023**, *8*, e202303271.
53. Yu H.-Z., Baskin J.S., Zewail A.H. *J. Phys. Chem. A* **2002**, *106*, 9845-9854.
54. Zheng F., Hsu C.S., Zhang Ya., Sun Yo., Wu Ya., Lu H., Sun X., Shi Q. *Energy Fuels* **2018**, *32*, 10382-10390.
55. Liu T., Li J., Zhao L.X., Zhou Ya., Wei Q., Xu C., Zhang Ya., Ding S., Zhang T., Tao X., Ju L., Shi Q. *Energy Fuels* **2015**, *29*, 2089-2096.
56. Koifman O.I., Rychikhina E.D., Travkin V.V., Sachkov Y.I., Stuzhin P.A., Somov N.V., Yunin P.A, Zhabanov Y.A., Pakhomov G.L. *ChemPlusChem* **2023**, *88*, e202300141.
57. Espinosa M., Pacheco U.S., Leyte F., Ocampo R. *J. Porphyrins Phthalocyanines* **2014**, *18*, 542-551.
58. Xu H., Que G., Yu D., Lu J.R. *Energy Fuels* **2005**, *19*, 517-524.
59. Xu H., Yu D., Que G. *Fuel* **2005**, *84*, 647-652.
60. Bird C.W. *Tetrahedron* **1985**, *41*, 1409-1414.
61. Eglinton G., Maxwell J.R., Evershed R.P., Barwise A.J.G. *Interdiscip. Sci. Rev.* **1985**, *10*, 222-236.

Received 01.10.2025
Accepted 08.12.2025